Enhancing the Photothermal Stability of Plasmonic Metal Nanoplates by a Core-Shell Architecture

*Xiaoqing Huang, Shaoheng Tang, Biju Liu, Bin Ren, and Nanfeng Zheng**

Over recent decades, metal nanostructures exhibiting distinct surface-plasmon-resonance (SPR) effects have attracted increasing attention due to their broad applications in the optical sensing of small molecules/biomolecules,[1,2] enhancing spectral signals,[3,4] probing catalytic reactions,[5] and photothermal therapy.[6–10] Through the extensive research efforts of many research groups, significant progress has been made in preparing novel metal nanostructures with tunable SPR properties.[6–13] Currently, these materials are mainly limited to Ag or Au. In order to have SPR tunability over a wide spectral region, particularly in the near-IR (NIR) region, the Au or Ag nanostructures need to be structurally anisotropic (e.g., nanorods, nanoplates)[10,11,14–17] or hollow (e.g., nanocages, nanoshells).[6,8,9] Upon irradiation by a strong laser, however, the heat generated from the photothermal effect often melts hollow or anisotropic Au/Ag nanostructures into solid spheres, resulting in poor photothermal stability and thus easy loss of their NIR-SPR properties.[18,19]

In contrast to Ag/Au, the chemical synthesis of Pd nanostructures that exhibit well-defined SPR has received limited success, although Pd nanodisks displaying tunable SPR features have been fabricated through lithography.[2,20] With the successful synthesis of freestanding, ultrathin Pd nanosheets, we recently demonstrated that nanostructured Pd can have well-defined NIR-SPR properties together with a significantly enhanced photothermal stability.[21] Unfortunately, the Pd nanosheets need to be ultrathin to have such well-defined SPR absorption features. Increasing the thickness of the 2D Pd nanostructures led to much-broader SPR peaks in the visible region.[22,23] The chemical synthesis of metal nanostructures having both SPR tunability and enhanced photothermal stability is still challenging.

By coating the ultrathin Pd nanosheets with Ag at different thickness, we now report here a seeded synthesis of a class of core-shell Pd@Ag nanostructures, integrating both tunable SPR properties and photothermal stability. In the synthesis, uniform hexagonal Pd nanoplates, 1.8 nm thick, are used as seeds to direct the epitaxial growth of Ag thereon. The thickness of the Ag layer can be chemically fine-tuned by the amount of Ag supplied. Profiting from the uniformity and outstanding photothermal stability of the Pd seeds, the prepared core-shell Pd@Ag platelets are uniform in both size and shape, and display significantly enhanced photothermal stability as compared with pure Ag nanostructures. The applications of the Pd@Ag nanoplates as a substrate for NIR surface-enhanced Raman scattering (NIR-SERS) and an NIR absorber for photothermal cancer therapy are also demonstrated.

In a typical preparation of the plasmonic Pd-Ag core-shell bimetallic nanoplates (see Experimental Section for details), hexagonal Pd nanosheets with an average edge length of 41 nm and a thickness of 1.8 nm were first synthesized in an aqueous solution of Pd(II) acetylacetonate ($Pd(acac)_2$) by utilizing carbon monoxide as a surface-confining agent and a reducing agent.[21] The obtained Pd nanosheets (Figure S1, Supporting Information) were then used as seeds for the formation of bimetallic Pd-Ag nanoplates by reducing $AgNO_3$ with methanal in an aqueous solution.

Representative transmission-electron-microscopy (TEM) images of the as-made bimetallic Pd-Ag nanoplates are shown in **Figure 1**. It is clearly revealed that the overall morphology of the bimetallic nanoplates adopted a hexagonal plate-like shape with a mean diameter (diagonal of the hexagon) of 83 nm (Figure 1a–c). The large-area TEM image (Figure S2, Supporting Information) shows that no isolated Ag nanoparticles were present in the products. As illustrated in the high-resolution TEM (HR-TEM) image (Figure 1d), the as-prepared, bimetallic, Pd-Ag nanoplates were highly crystalline, showing well-defined lattice fringes. The detected lattice fringes had a *d*-spacing of 2.38 Å, which corresponds to the 1/3{422} planes of face-centered-cubic (fcc) Ag (Figure S3, Supporting Information). Moreover, the elemental distribution of the Ag atoms on the surface of the Pd nanosheets was studied by energy-dispersive X-ray (EDX) spectroscopy. Both the EDX line profile (Figure 1e) and the elemental-mapping analysis (Figure 1f) revealed that Ag and Pd atoms were both homogeneously distributed throughout the as-prepared core-shell Pd-Ag nanoplates, suggesting that the Ag was epitaxially grown on the Pd.

Even with the epitaxial growth of Ag and thus the increased thickness, it should be noted that the obtained Pd@Ag core-shell nanoplates kept the original diameter of the Pd seeds. As many previous studies have demonstrated, the SPR properties of 2D metal nanoplates highly depend on their aspect ratio (the diameter-to-thickness ratio).[24,25] We thus attempted to prepare Pd@Ag nanoplates with different thicknesses by supplying different amounts of Ag to the same amount of Pd seeds. The thickness of the Pd@Ag nanoplates increased from 3.5 to 5.4, 6.9, 9.9, 14.1, and 19.8 nm when the Ag/Pd molar ratio was increased from 1.8 to 2.7, 3.6, 5.4, 7.3 and 11.0, respectively (see Figure S4, Supporting Information for TEM images). The elemental distributions studied by EDX also revealed that both the Pd and the Ag were homogenously distributed in

X. Q. Huang, S. H. Tang, B. J. Liu, Prof. B. Ren, Prof. N. F. Zheng
State Key Laboratory for Physical Chemistry of Solid Surfaces and Department of Chemistry
College of Chemistry and Chemical Engineering
Xiamen University
Xiamen 361005, China
E-mail: nfzheng@xmu.edu.cn

DOI: 10.1002/adma.201100905

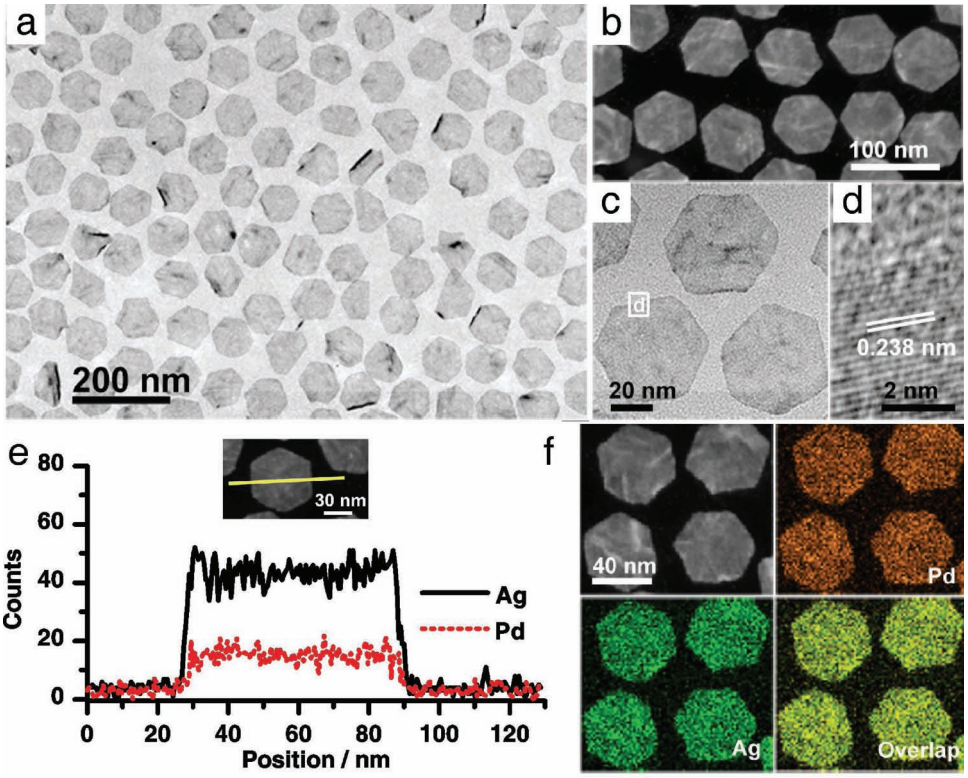

Figure 1. a) Representative large-area TEM image. b) High-angle annular dark-field scanning transmission electron microscopy (HAADF-STEM) image. c) Enlarged TEM image of the plasmonic Pd@Ag core-shell bimetallic nanoplates. d) High-resolution TEM image of the square area indicated in Figure 1c. e) HAADF-STEM image and EDX line profiles of a Pd@Ag nanoplate. f) EDX mapping images of the Pd@Ag nanoplates. The Pd@Ag nanoplates had a Ag/Pd molar ratio of 1.8.

all of the obtained core-shell nanoplates (Figure S5–S6, Supporting Information). While the thickness increased with the supplied Ag amount (Figure S3), the diameters of the obtained nanoplates were all narrowly distributed around 85 nm. As a result, the aspect ratio (the diameter-to-thickness ratio) of the obtained Pd@Ag nanoplates decreased with the increase of the Ag content. Such a change of aspect ratio explains well the different colors of the products that were yielded with the different Ag/Pd ratios (**Figure 2**a). When the Ag/Pd ratio was 1.8, the resulting solution appeared to be green. The color of the products changed to blue-green, blue, purple and yellow when the Ag/Pd atomic ratio increased to 2.7, 3.6, 5.4, 7.3 and 11.0, respectively. Accordingly, as shown in Figure 2b, the maximum optical absorption of the resulted solution was blue-shifted from 971 to 812, 710, 602, 529 and 477 nm when the Ag/Pd ratio was increased from 1.8 to 2.7, 3.6, 5.4, 7.3 and 11.0, respectively.

Having a uniform size and morphology, the Pd@Ag nanoplates prepared by the seeding method reported here nicely inherited the uniformity of the Pd seed nanosheets. To compare the photothermal stability of our Pd@Ag core-shell nanoplates with that of 2D, pure-Ag nanostructures, we chose the Pd@Ag nanoplates that had a thickness of 5.4 nm and prepared triangular silver nanoprisms according to a method described in the literature for comparison.[24] As shown in **Figure 3**, before the laser irradiation, both our Pd@Ag nanoplates and the Ag nanoprisms showed NIR SPR with maximum absorptions at 812 and 753 nm, respectively. However, after irradiation for 30 min by a

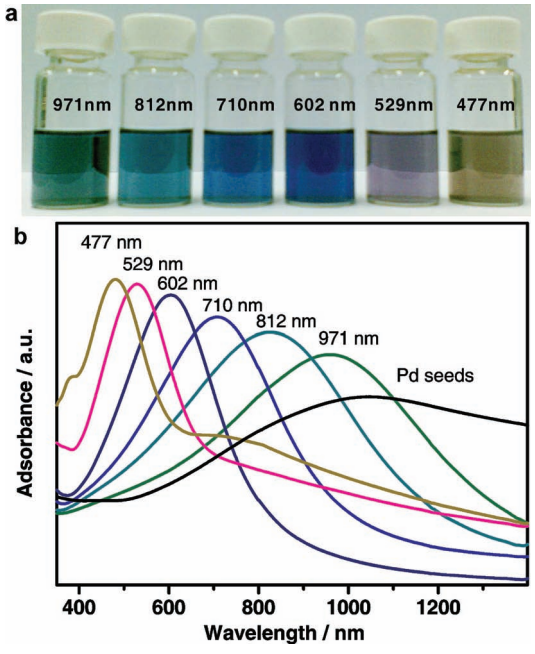

Figure 2. a–b) Digital photographs (a) and corresponding extinction spectra (b) showing the precise tuning of the plasmon bands of the Pd@Ag core-shell bimetallic nanoplates by varying the $AgNO_3$/Pd nanoplates' molar ratio. From left to right, the samples in Figure 2a were prepared using $AgNO_3$/Pd ratios of 1.8, 2.7, 3.6, 5.4, 7.3 and 11.0, respectively.

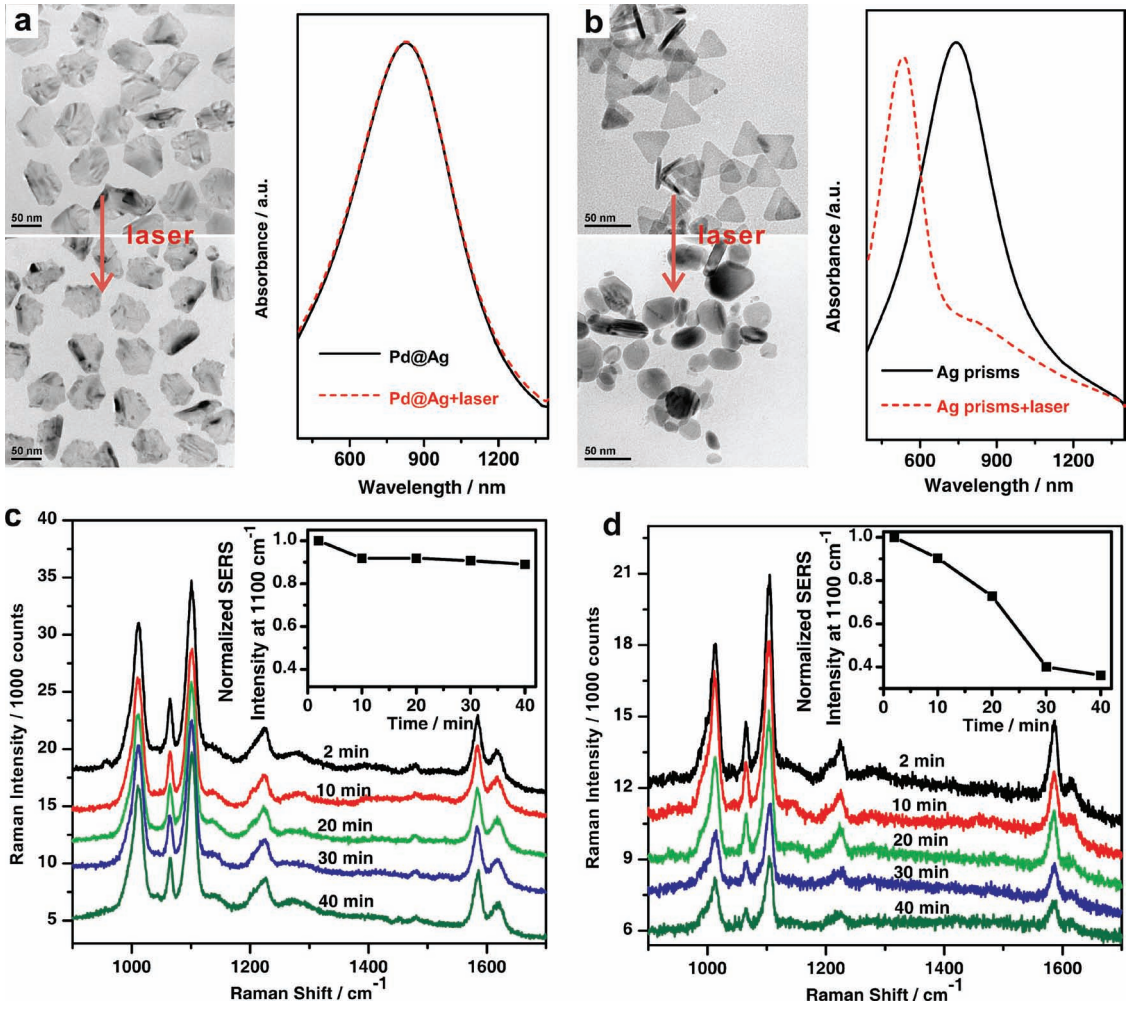

Figure 3. a–b) Comparison of the photothermal stability of the plasmonic Pd@Ag core-shell bimetallic nanoplates (a) and Ag nanoprisms (b) upon irradiation for 30 min with a 2 W, 808 nm laser. In Figure 3a and 3b, the top-left and bottom-left images are TEM images of the nanoparticles before and after the laser irradiation, respectively. The SPR changes of the nanoparticles after the laser irradiation are shown on the right-hand side of Figure 3a and 3b. c–d) SERS spectra of 4-pyridinethiol recorded from: the plasmonic Pd@Ag core-shell bimetallic nanoplates (c) and the Ag nanoprisms (d), upon different laser irradiation times. The insets in Figure 3c and 3d show the normalized Raman intensity at the 1100 cm^{-1} peak versus the laser-irradiation time.

2 W, 808 nm laser, while the absorption spectrum of the pure Ag solution showed a significant blue-shift of the maximum peak to 530 nm, the Pd@Ag core-shell nanoplates displayed no notable change in their absorption. Indeed, as revealed by the TEM studies, the significant blue-shift of the pure Ag nanoprisms was due to the change of their 2D structure upon irradiation. In comparison, the irradiated Pd@Ag core-shell nanoplates nicely retained their 2D structure (Figure S2d, Supporting Information). This result suggests that the presence of the Pd nanosheet at the core significantly enhanced the photothermal stability of the Pd@Ag nanoplates. As we have previously demonstrated, Pd nanosheets alone display extraordinary photothermal stability upon NIR laser irradiation, which has been impossible to realize with pure-Ag nanoplates. It is well documented in the literature that Ag can grow epitaxially on Pd at a temperature of up to 500 K.[26] According to the method proposed by de Abajo et al., the use of a continuous-wave laser with a power density of 1.4 W cm^{-2} in our photothermal studies creates a negligible temperature difference between the metal nanoplates and the surrounding water.[27] Therefore, the enhanced stability of the Pd@Ag nanoplates can be explained by the high photothermal stability of the core Pd sheet together with its strong interaction with the Ag shell.

The NIR-SPR properties of the as-prepared Pd@Ag nanoplates are greatly preserved even after irradiation by a high-power laser, which should be critical for many potential applications, such as NIR surface-enhanced Raman scattering (NIR-SERS)[28–32] and photothermal cancer therapy.[6–10] To demonstrate the advantages of Pd@Ag over 2D, pure-Ag nanostructures as the substrate for NIR-SERS, we carried out measurements in situ by monitoring the Raman signals of 4-pyridinethiol on both the Pd@Ag nanoplates and the Ag nanoprisms, while keeping the NIR irradiation on the samples (see Experimental Section for details). As clearly shown in

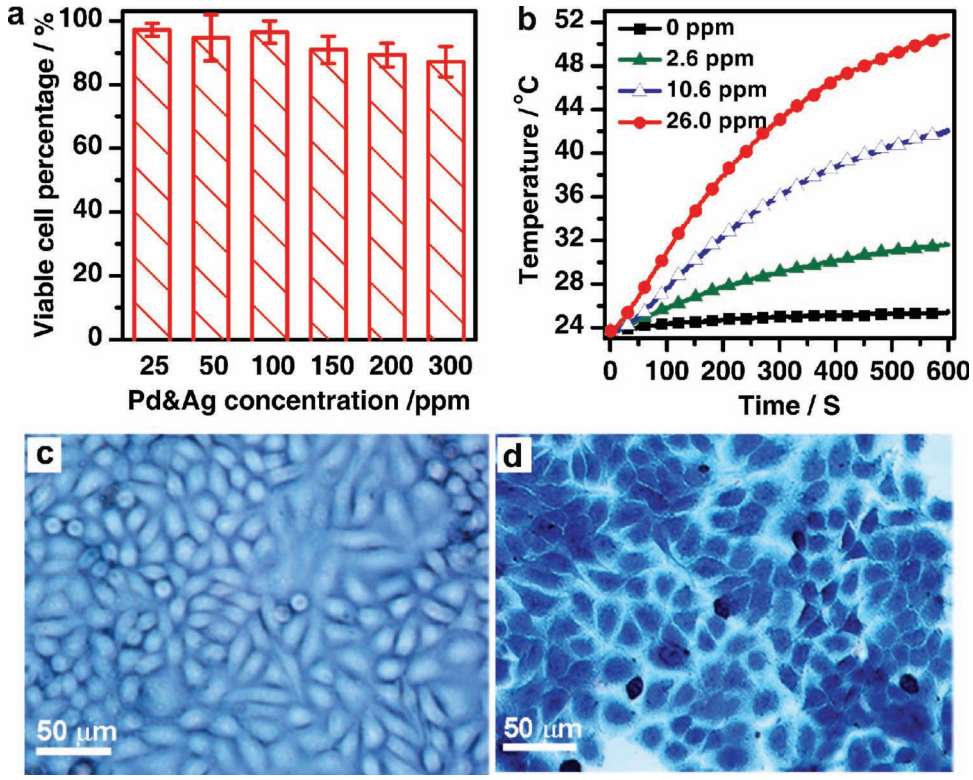

Figure 4. a) Viability of healthy liver cells incubated for 48 h with different concentrations of silica-coated Pd@Ag nanoplates. b) Photothermal effect of the silica-coated Pd@Ag nanoplates. Temperature–time plots were recorded for various concentrations of Pd@Ag nanoplates upon irradiation by a 1 W laser. c–d) Micrographs of cancer cells under irradiation for 0 min after incubation with silica coated Pd@Ag nanoplates (20 μg mL^{-1}) (c), and irradiation for 5 min with a 2 W, 808 nm laser after incubation with the silica-coated Pd@Ag nanoplates (20 μg mL^{-1}) (d). The silica-coated Pd@Ag nanoplates had a core thickness of 5.4 nm (Pd@Ag nanoplates) and a shell thickness of 38 nm (silica). The power density was 1.4 W cm^{-2}. Dead cells are stained with Trypan Blue.

Figure 3c–d, the SERS signals of the 4-pyridinethiol on Pd@Ag were well maintained under the laser irradiation (785 nm, 12 mW). After irradiation for 40 min, the signals decreased by less than 10%. In comparison, the signals on the Ag nanoprisms dramatically decreased on prolonging the irradiation time. There was as much as 60% decay in the signals after irradiation for 40 min. These results suggest that the excellent photothermal stability of the core-shell Pd@Ag nanoplates might make them potentially useful and reliable substrates for SERS applications.

The strong SPR absorption of the core-shell Pd@Ag nanoplates in the NIR region also motivated us to investigate the potential of these nanoplates in photothermal cancer therapy using an NIR laser. Pd@Ag nanoplates having a thickness of 5.4 nm were chosen for the photothermal-therapy studies. As compared to pure Pd nanosheets, the biocompatibility of the as-prepared Pd@Ag nanoplates was somewhat reduced (Figure S7, Supporting Information). We therefore coated the Pd@Ag nanoplates with a layer of silica to improve their biocompatibility (**Figure 4**a and Figure S8, Supporting Information). While enhancing their biocompatibility, the silica coating altered neither the NIR-SPR properties nor the photothermal effect of the Pd@Ag nanoplates (Figure 4b, Figure S9, Supporting Information). The photothermal effect of the silica-coated nanostructures was investigated by monitoring the temperature of 1 mL of an aqueous solution of the Pd@Ag nanoplates irradiated by a NIR laser (808 nm, 1 W). The temperature of the solution containing 26 ppm Pd/Ag was raised from 23.7 to 50.8 °C after irradiation for 10 min. In comparison, the temperature of the solution in the absence of the bimetallic nanostructures was increased by only 0.4 °C (Figure 4b). Such a photothermal effect induced by the NIR SPR absorption was enough to induce thermal damage to the targeted tissue. After being incubated with silica-coated Pd@Ag nanoplates, ~100% of the liver cancer cells were killed after irradiation for 5 min with an 808 nm laser providing a power density of 1.4 W cm^{-2} (Figure 4d): the photothermal cell-killing efficacy of the silica-coated Pd@Ag nanoplates is comparable or even higher than other reported results.[33–35] In comparison, neither the silica-coated Pd@Ag nanoplates nor the laser irradiation alone killed the cancer cells (Figure 4c and Figure S10, Supporting Information).

In summary, plasmonic Pd@Ag core-shell nanoplates were successfully prepared in high yields using uniform Pd nanosheets as the seeds. The bimetallic nanoplates exhibited tunable SPR properties over a wide spectral range and outstanding photothermal stability relative to 2D, pure-Ag nanoprisms. Owing to the enhanced photothermal stability, we have also demonstrated the advantage of the core-shell nanoplates over the pure-Ag nanostructure as an NIR-SERS substrate. The prepared bimetallic nanoplates were used as effective NIR

absorbers for photothermal cancer therapy. It is expected that the Pd@Ag core-shell bimetallic nanoplates reported herein could find more applications.

Experimental Section

Chemicals and Materials: $Pd(acac)_2$ (99%) was purchased from Alfa Aesar; $AgNO_3$ (A.R.), poly(vinylpyrrolidone) (PVP) (molecular weight (MW) = 30 000 g mol^{-1}), *N*, *N* -dimethylformamide (DMF) (A.R.), methanal solution (40%), and tetrabutylammonium bromide (TBAB) were purchased from Sinopharm Chemical Reagent Co. Ltd. (Shanghai, China). The water used in all of the experiments was ultrapure (18.2 M cm^{-1}). All of the reagents were used as received without further purification.

Synthesis of Hexagonal Pd Nanoplates: In a typical synthesis of the hexagonal Pd nanoplates, $Pd(acac)_2$ (50.0 mg), PVP (MW = 30 000 g mol^{-1}, 160.0 mg) and TBAB (185 mg) were mixed together with DMF (10.0 mL) and water (2.0 mL). The resulting homogeneous yellow solution was transferred to a glass pressure vessel. The vessel was then charged with CO to 1 bar and heated at 100 °C for 3.0 h before being cooled to room temperature. The dark-blue colloid solution was directly used as a seed solution for further synthesis of the bimetallic Pd@Ag core-shell nanoplates.

Synthesis of the Plasmonic Pd@Ag Core-Shell Bimetallic Nanoplates: A solution (0.10 mL) of the Pd nanoplates produced as above was purified with an ethanol (1 mL)-acetone (8 mL) mixture once to remove excessive surfactants and ions. The purified Pd nanoplates were then redispersed in water (4.0 mL). A desired amount (i.e., a: 0.10 mL, b: 0.15 mL, c: 0.20 mL, d: 0.30 mL, e: 0.40 mL or f: 0.60 mL) of $AgNO_3$ (0.025 M) solution and methanal solution (0.50 mL, 40%) were then added to the Pd-nanoplates solution in turn. The mixture was stirred vigorously for 1 min, and then left undisturbed at room temperature for about 10 h. The products were precipitated with acetone, separated via centrifugation at 14 000 rpm and further purified twice with an ethanol (1 mL)-acetone (8 mL) mixture.

Synthesis of Silica-Coated Bimetallic Pd@Ag Core-Shell Nanoplates: Typically, ethanol (16.0 mL) and methylamine solution (0.50 mL, 40%) were added to a solution (2.0 mL) of unpurified bimetallic Pd@Ag core-shell nanoplates. After stirring for 30 min, tetraethoxysilane (TEOS) ethanol solution (1.0 mL, 1% TEOS, volume ratio) was added. The reaction mixture was further stirred for 8 h. The resultant colloids were precipitated by acetone, separated via centrifugation at 14 000 rpm and further purified twice with an ethanol-acetone mixture.

Characterization: The TEM (including the HR-TEM) studies were performed using a TECNAI F-30 high-resolution transmission electron microscope operating at 300 kV. The samples were prepared by dropping ethanol dispersions of the samples onto 300-mesh carbon-coated copper grids and immediately evaporating the solvent. SEM studies were performed using a Hitachi S4800 scanning electron microscope with a field-emission electron gun. The samples were prepared by dropping ethanol dispersions of the samples onto Si substrates and immediately evaporating the solvent.

Surface-Enhanced Raman Scattering (SERS) Experiments: The 4-pyridinethiol-modified samples were prepared for SERS experiments by exchanging the Pd@Ag with 5 mL of 4-pyridinethiol in a 20×10^{-3} M ethanolic solution, which was stirred for 2 h at room temperature. After thorough rinsing, the samples were dropped onto silicon wafers and dried under room temperature. All of the SERS experiments were carried out using a 50× objective lens (numeric aperture (NA) = 0.55) and the spectra were taken using an acquisition time of 10 s, between 900 and 1700 cm^{-1}. The laser was a 785 nm diode laser.

Photothermal-Effect Measurement: To study the photothermal effect induced by the NIR-SPR absorption, an aqueous solution (1 mL) of the silica-coated plasmonic Pd@Ag core-shell nanoplates was irradiated using an NIR laser (808 nm, 1 W). The temperature of the solution was monitored using a submerged thermocouple microprobe. The photothermal stability of the plasmonic Pd@Ag core-shell nanoplates was studied by irradiating the plasmonic-nanoplate solution with a 2 W, 808 nm laser for 30 min.

Apoptosis Assay: Healthy human liver cells were cultured in Roswell Park Memorial Institute (RPMI) 1640 medium in 24-well plates. The cell density was 1×10^5 cells per well. After being seeded for 18 h, the RPMI 1640 medium was replaced with culture media containing different concentrations of the silica-coated plasmonic Pd@Ag core-shell nanoplates. The incubations were carried out at 37 °C in 5% CO_2 atmosphere for 48 h. After incubation for 48 h, the cell viabilities were measured by a standard 3-(4,5-dimethylthiazol-2-yl)-2,5-diphenyltetrazolium bromide (MTT) assay.

In Vitro Photothermal Therapy: Human hepatocytes were cultured in RPMI 1640 medium in 24-well plates. The cell density was 5×10^5 cells per well. Before incubation with the silica-coated plasmonic Pd@Ag core-shell nanoplates, the cells were seeded for 18 h. Silica-coated plasmonic Pd@Ag core-shell nanoplates in water were added to each well at a concentration of 20 mg mL^{-1}. The incubations were carried out at 37 °C in 5% CO_2 atmosphere for 12 h. After incubation, the cell medium was removed, and the cells were washed twice before a phosphate-buffered-saline (PBS) buffer solution was added. After incubation with the plasmonic nanoplates, the human hepatocytes were exposed to a 2 W, 808 nm laser for various periods to induce photothermal cell damage. To identify the cell viability, the dead cells were stained with Trypan Blue.

Supporting Information

Supporting Information is available from the Wiley Online Library or from the author.

Acknowledgements

We thank the NSFC (21021061, 20925103, 20923004, 20871100), the Fok Ying Tung Education Foundation (121011), the MOST of China (2011CB932403, 2009CB930703), the NSF of Fujian Province (Distinguished Young Investigator Grant 2009J06005), and the Key Scientific Project of Fujian Province (2009HZ0002-1) for their financial support.

Received: March 10, 2011
Revised: May 16, 2011
Published online: June 20, 2011

[1] R. Gordon, D. Sinton, K. L. Kavanagh, A. G. Brolo, *Acc. Chem. Res.* **2008**, *41*, 1049.
[2] C. Langhammer, Z. Yuan, I. Zoric, B. Kasemo, *Nano Lett.* **2006**, *6*, 833.
[3] N. Calander, *Curr. Anal. Chem.* **2006**, *2*, 203.
[4] A. M. Gobin, M. H. Lee, N. J. Halas, W. D. James, R. A. Drezek, J. L. West, *Nano Lett.* **2007**, *7*, 1929.
[5] E. M. Larsson, C. Langhammer, I. Zoric, B. Kasemo, *Science* **2009**, *326*, 1091.
[6] S. Lal, S. E. Clare, N. J. Halas, *Acc. Chem. Res.* **2008**, *41*, 1842.
[7] P. K. Jain, X. H. Huang, I. H. El-Sayed, M. A. El-Sayed, *Acc. Chem. Res.* **2008**, *41*, 1578.
[8] S. E. Skrabalak, J. Y. Chen, Y. G. Sun, X. M. Lu, L. Au, C. M. Cobley, Y. N. Xia, *Acc. Chem. Res.* **2008**, *41*, 1587.
[9] M. Hu, J. Y. Chen, Z. Y. Li, L. Au, G. V. Hartland, X. D. Li, M. Marquez, Y. N. Xia, *Chem. Soc. Rev.* **2006**, *35*, 1084.
[10] X. H. Huang, S. Neretina, M. A. El-Sayed, *Adv. Mater.* **2009**, *21*, 4880.
[11] C. J. Murphy, T. K. San, A. M. Gole, C. J. Orendorff, J. X. Gao, L. Gou, S. E. Hunyadi, T. Li, *J. Phys. Chem. B* **2005**, *109*, 13857.
[12] P. K. Jain, X. Huang, I. H. El-Sayed, M. A. El-Sayad, *Plasmonics* **2007**, *2*, 107.

[13] J. Perez-Juste, I. Pastoriza-Santos, L. M. Liz-Marzan, P. Mulvaney, *Coord. Chem. Rev.* **2005**, *249*, 1870.
[14] R. C. Jin, Y. W. Cao, C. A. Mirkin, K. L. Kelly, G. C. Schatz, J. G. Zheng, *Science* **2001**, *294*, 1901.
[15] R. C. Jin, Y. C. Cao, E. C. Hao, G. S. Metraux, G. C. Schatz, C. A. Mirkin, *Nature* **2003**, *425*, 487.
[16] E. Carbo-Argibay, B. Rodriguez-Gonzalez, J. Pacifico, I. Pastoriza-Santos, J. Perez-Juste, L. M. Liz-Marzan, *Angew. Chem. Int. Ed.* **2007**, *46*, 8983.
[17] J. Perez-Juste, B. Rodriguez-Gonzalez, P. Mulvaney, L. M. Liz-Marzan, *Adv. Funct. Mater.* **2005**, *15*, 1065.
[18] S. Link, C. Burda, M. B. Mohamed, B. Nikoobakht, M. A. El-Sayed, *J. Phys. Chem. A* **1999**, *103*, 1165.
[19] M. S. Yavuz, Y. Y. Cheng, J. Y. Chen, C. M. Cobley, Q. Zhang, M. Rycenga, J. W. Xie, C. Kim, K. H. Song, A. G. Schwartz, L. H. V. Wang, Y. N. Xia, *Nat. Mater.* **2009**, *8*, 935.
[20] C. Langhammer, B. Kasemo, I. Zoric, *J. Chem. Phys.* **2007**, *126*, 194702.
[21] X. Q. Huang, S. H. Tang, X. L. Mu, Y. Dai, G. X. Chen, Z. Y. Zhou, F. X. Ruan, Z. L. Yang, N. F. Zheng, *Nature Nanotechnol.* **2011**, *6*, 28.
[22] Y. J. Xiong, I. Washio, J. Y. Chen, H. G. Cai, Z. Y. Li, Y. N. Xia, *Langmuir* **2006**, *22*, 8563.
[23] Y. J. Xiong, J. M. McLellan, J. Y. Chen, Y. D. Yin, Z. Y. Li, Y. N. Xia, *J. Am. Chem. Soc.* **2005**, *127*, 17118.
[24] G. S. Metraux, C. A. Mirkin, *Adv. Mater.* **2005**, *17*, 412.
[25] Q. Zhang, J. P. Ge, T. Pham, J. Goebl, Y. X. Hu, Z. Lu, Y. D. Yin, *Angew. Chem. Int. Ed.* **2009**, *48*, 3516.
[26] C. Felix, G. Vandoni, W. Harbich, J. Buttet, R. Monot, *Phys. Rev. B: Condens. Matter* **1996**, *54*, 17039.
[27] G. Baffou, R. Quidant, F. J. G. de Abajo, *ACS Nano* **2010**, *4*, 709.
[28] F. Casadio, M. Leona, J. R. Lombardi, R. Van Duyne, *Acc. Chem. Res.* **2010**, *43*, 782.
[29] K. Kneipp, H. Kneipp, R. Manoharan, I. Itzkan, R. R. Dasari, M. S. Feld, *J. Raman Spectrosc.* **1998**, *29*, 743.
[30] J. P. Camden, J. A. Dieringer, J. Zhao, R. P. Van Duyne, *Acc. Chem. Res.* **2008**, *41*, 1653.
[31] X. M. Qian, X. H. Peng, D. O. Ansari, Q. Yin-Goen, G. Z. Chen, D. M. Shin, L. Yang, A. N. Young, M. D. Wang, S. M. Nie, *Nat. Biotechnol.* **2008**, *26*, 83.
[32] M. Sanles-Sobrido, W. Exner, L. Rodriguez-Lorenzo, B. Rodriguez-Gonzalez, M. A. Correa-Duarte, R. A. Alvarez-Puebla, L. M. Liz-Marzan, *J. Am. Chem. Soc.* **2009**, *131*, 2699.
[33] L. R. Hirsch, R. J. Stafford, J. A. Bankson, S. R. Sershen, B. Rivera, R. E. Price, J. D. Hazle, N. J. Halas, J. L. West, *Proc. Natl. Acad. Sci. USA* **2003**, *100*, 13549.
[34] X. H. Huang, I. H. El-Sayed, W. Qian, M. A. El-Sayed, *J. Am. Chem. Soc.* **2006**, *128*, 2115.
[35] J. Y. Chen, D. L. Wang, J. F. Xi, L. Au, A. Siekkinen, A. Warsen, Z. Y. Li, H. Zhang, Y. N. Xia, X. D. Li, *Nano Lett.* **2007**, *7*, 1318.